ASSOCIAÇÃO PORTUGUESA DOS RECURSOS HÍDRICOS

EXPERIMENTAL AND NUMERICAL SIMULATIONS OF OBLIQUE EXTREME WAVE CONDITIONS IN FRONT OF A BREAKWATER'S TRUNK AND ROUND HEAD

R.F. Carvalho[@ 1], J.A. Santos[2], G. Barajas Ojeda[3], Md. N.A. Beg[1], P.M. Lopes[1], J.C. Fortes[4], J. L. Lara[3]

ABSTRACT: Climate change studies already reported sea level rise as an accepted scenario, which induces changes in nearshore wave conditions. A large range of new experiences including water level, run-up, overtopping, hydrodynamic data for different wave steepnesses and directions was performed in the Leibniz Universität Hannover (LUH) wave basin for a rubble mound breakwater with a slope of 1(V):2(H). This work presents, focusing on oblique extreme wave conditions, numerical simulations of the hydrodynamics in that experiment using OpenFOAM®. Results of the wave generation boundary conditions and their propagation, namely elevation of the water level free-surface and velocity data at specific locations are compared and discussed with data from experimental measurements acquired by acoustic wave gauges and acoustic doppler velocimeter (ADV) / Vectrino equipment. Although an exact match between numerical and laboratory values was not reached, an appropriate incident wave angle and a reasonable amplitude of velocities and water depths was achieved and the same happened to the statistics of those values.

Keywords: breakwater, wave generation, OpenFOAM®, scale-model tests, oblique extreme wave conditions.

RESUMO: A estimativa do impacto de cenários de alterações climáticas em quebra-mares de taludes é fundamental para a gestão e manutenção dessas obras. Foram realizados ensaios no tanque de ondas de Leibniz Universität Hannover (LUH), para avaliar o comportamento de um quebra-mar de taludes com uma inclinação de 1 (V): 2 (H), quando sujeito à incidência de condições de agitação marítima e níveis de maré extremos, resultantes desses cenários de alterações climáticas. Foram efetuadas simulações numéricas dos ensaios efetuados. Este trabalho apresenta em particular, simulações numéricas da hidrodinâmica dos ensaios com foco em condições de ondas extremas oblíquas, usando OpenFOAM®. Foram reproduzidas as condições de fronteira de geração de onda e analisado os resultados da sua propagação, a elevação da superfície livre e dados de velocidade em locais específicos que são comparados e discutidos com dados de medidas experimentais adquiridas por medidores de ondas acústicas e velocímetro doppler acústico (ADV) / Equipamento Vectrino. Embora uma correspondência exata entre os valores numéricos e laboratoriais não tenha sido alcançada, um ângulo de onda incidente apropriado e uma amplitude razoável de velocidades e profundidades de água foram alcançados e o mesmo aconteceu com as estatísticas desses valores.

Palavras-chave: quebra-mar, geração de ondas, OpenFOAM®, testes em modelo reduzido, condições de ondas extremas oblíquas.

@   Corresponding author: ritalmfc@dec.uc.pt

1   MARE, Dep. Civil Engineering, University of Coimbra, Coimbra, Portugal

2   ISEL – Instituto Superior de Engenharia de Lisboa, Instituto Politécnico de Lisboa, Lisboa, Portugal. E-mail: jasantos@dec.isel.ipl.pt

3   IHCantabria, Instituto de Hidraulica Ambiental, Universidad de Cantabria, Santander, Spain. E-mail: gabriel.barajas@unican.es

4   LNEC – National Laboratory of Civil Engineering, Lisboa Portugal. E-mail: jfortes@lnec.pt

1. INTRODUCTION

The influence of high incidence angles (very oblique waves) on breakwaters is unknown, as limited data is available. The accepted climate change scenarios, which report sea level rise (Weisse *et al*., 2014), causing different conditions of incident wave angles on breakwaters, foster the study of very oblique waves in what concerns both their characterization as well as their influence on rubble-mound breakwaters within RodBreak experimental work (Santos *et al*., 2019a). RodBreak main goal was to contribute to a new whole understanding of the phenomena filling existing data gaps in the R&D&I, to enable the mitigation of future sea level rise in European coastal structures (Santos *et al*., 2019b). This includes the run-up and overtopping characterization on rough and permeable slopes, as well as to check and extend the validity range of the formulas developed for armour layer stability, focusing on oblique extreme wave conditions and on their effects on a gentler slope breakwater's trunk and roundhead.

On the other hand, over the last decades, Navier-Stokes numerical models have been developed to accurately simulate wave interaction with all kinds of coastal structures, which allows the study of a vast number of three-dimensional effects. WAVE2FOAM (Jacobsen *et al*., 2012) and IH-FOAM (Higuera *et al*., 2013) have been applied to study waves in channels and basins at laboratory and prototype scale, simulating different types of waves.

IHFOAM, which is included in OpenFOAM® V18.12, was applied to study interactions of a regular wave train generated with different angles with a vertical breakwater inducing three-dimensional wave patterns. Lara *et al*. (2012), assumed a boundary condition perpendicular to wave train direction to better represent the correct direction. This procedure is not convenient on extremely oblique wave train in tanks, because to make the correct direction, the walls and dimensions of the tank have to be profoundly altered.

This work aims to reproduce through numerical simulations the conditions of the wave verified in experiments, in order to allow the analysis of the influence of oblique waves in the wave propagation, run-up, breaking and overtopping, and their impact in the stability of rubble mound breakwaters (water layer thickness and velocities). We present a preliminary work to show the range of applicability of a three-dimensional Navier-Stokes model and the boundary conditions to generate oblique wave trains, to propagate in the basin with a rubble mound

breakwater with a slope of 1(V):2(H). We compare numerical data with experimental measurements of free-surface elevation and velocities along time and their statistics. The work is organized as follows: the experimental work and the numerical model are presented in section 2 and 3, respectively. Focusing on wave generation and propagation, results of numerical simulations and measurement are presented in section 4. Both measurements and numerical wave data are discussed and compared in section 5 and conclusions are summarized and presented in section 6.

2. EXPERIMENTAL WORK

Experimental Installation

The experimental work was performed at the Marienwerder facilities of the Leibniz University, Hannover (LUH). A stretch of a rubble mound breakwater (head and part of the adjoining trunk), with a slope of 1(V):2(H) was built in the wave basin to be reached by different extreme wave conditions (wave steepness of 0.055) with incident irregular wave train angles from 40º to 90º.

Figure 1 presents a perspective view of the breakwater model, and schematics of the structure and its cross section. The trunk of the breakwater is 7.5 m long, and the head has the same cross section as the exposed part of breakwater. The total model length, measured along the crest axis, is 9.3 m, the model height is 0.83 m and its width is 3.7 m.

The construction of the model used a mould to ensure the desired alignment for the axis as well as for the several layers of the model. The core (15 m³) was made of gravel with a median weight 58.84 N and the filter layer, placed on top of the core, was made of gravel with a median weight of 578.60 N. Antifer cubes with a weight of 3442.19 N were deployed in two layers at the armour layer of both the breakwater head and at the 2.5 m wide adjoining strip of the breakwater trunk. It was expected the porosity of the armour layer to be 37%. Gravel with a median weight of 3089.14 N was employed both at the exposed and lee parts of the rock armour layer. The model was built with its axis making an angle of 70º with the main side of the basin. In the opposite wall it is located the wavemaker with 72 paddles.

All other tank walls contain fixed passive absorption devices made of a set of vertical mesh panels at different distances from the basin wall which act as vertical perforated screens, to
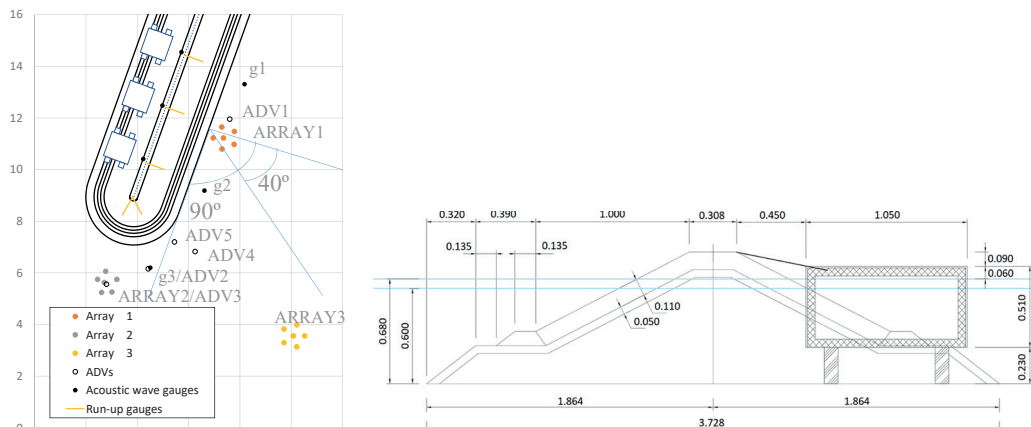
Figure 1. Plan view and cross-section of the model breakwater.

minimize unwanted wave reflections in the basin which allows to verify sea waves generated by the wavemaker, as well as the incident and reflected sea waves on the structure.

One wave gauge array was deployed in front of the wavemaker, another in front of the breakwater head, aligned with the breakwater crest, and one approximately at the middle of the breakwater trunk, in front of the entrance to the second overtopping reservoir.

Two additional isolated acoustic wave gauges were deployed in front of the entrance to the first and third overtopping reservoirs and a third in front the breakwater head, approximately in the middle of the dihedral angle formed with the vertical plane that marks the end of the trunk and the plan that contains the middle of the breakwater crest.

Generally, instrumentation was numbered starting from the root of the breakwater (gauge 1 is closer to the root of the breakwater and further away from the wavemaker). Exception was for ADV4 and ADV5, that were installed later. Additionally, capacitive wave gauges, 0.87 m long, were deployed over the armour layer to measure wave run-up, at the breakwater trunk, close to the sections where wave overtopping was to be measured, and at the breakwater head (one in the plan that contains the breakwater axis and the other was deployed perpendicularly to it).

Velocities were measured using five Vectrino instruments, which use Acoustic Doppler Velocimetry (ADV), deployed close to the breakwater to characterize the wave-induced flow. Three of them were deployed close to acoustic wave probes, to have an alternative source of information to compute the incident and reflected sea waves.

The remaining two Vectrinos were placed approximately on the vertical plane that marks the end of the breakwater trunk. Despite the difference between the vertical positions of the acoustic transmitter of the several Vectrinos, the acoustic receivers that define the x axis were all aligned with the breakwater crest. Table 1 presents the exact position of the probes, acoustic wave gauges and the Vectrinos/ADV equipment used in this work.

The z coordinate is measured above the bottom of the tank. All the electronic measuring equipment, apart from the Vectrinos, was connected to the same data acquisition device, which enable the creation of a single file of measured data per test with data from 35 sensors (18 acoustic wave gauges in 3 arrays of 6, 6 additional acoustic wave gauges for either the isolated measurement of the waves close to the model breakwater (3) or to detect overtopping events (3), 8 capacitive wave gauges either for run-up measurement (5) or water-level measurement inside the overtopping tanks (3) and 3 load cells to measure the overtopped volume).

These data was sampled at a 300 Hz rate. The ADV equipment /Vectrinos were directly connected to another computer and their recording was triggered by one of the Vectrinos, ensuring synchronization of all ADV equipment and velocity measurements, which were carried out at a rate of 100 Hz. Just one data file per Vectrino was produced for each test

2.3. Experimental Procedure and data analysis procedure

Table 2 shows the sequence of the tests for the long-crested waves (0º spread) with water depth of 0.60 m, which comprises different incidence wave angles (40º to 90º) and the parameters of each test.

For each test sequence, for a given water depth and incident direction, it was possible to carry out at least 4 tests for different wave conditions on the model (Hs=0.100 m, 0.150 m, 0.175 m and 0.200 m and the corresponding peak periods Tp=1.19 s, 1.45 s, 1.57 s and 1.68 s).

Gauges as well as ADV/Vectrino data, which was converted to ".dat" files using Vectrino Plus software, were analysed by several interconnected Matlab code files as follows:

1. DataGauges.mat - reads files ".txt", plot and calculates several statistics such as average and standard deviation as well as histograms and boxplots;

2. DataVectrino.mat – reads files ".dat" from Vectrino software conversion and prepare data to plot original and filtered data as variation along time, histograms, and boxplots, according:

    a.   correlation - DataCorrelationNoise.mat;

    b.   SNR analysis - DataSNRNoise.mat;

    c.   Goring and Nikora (2002) procedure extended by Wahl (2003) - DataElipsoide.mat;

    d.   DataVectrinobasicPlot;

3. DataVectrinoCalculus.mat, computes several parameters as velocity components average, standard deviation, and statistics as well as turbulence characteristics, saving them in files;

4. DataVectrinoPlot.mat, groups values in multiple locations along a line (longitudinal, profile) or a plane to plot.

Table 1. Coordinates of the acoustic wave gauges in the arrays, additional acoustic wave gauges and the Vectrinos (acoustic doppler velocimetry ADV).

Array acoustic wave gauges	probe	x(m)	y(m)
ARRAY1	1.1	-2.71	11.65
	1.2	-3.05	11.23
	1.3	-2.70	10.80
	1.4	-2.23	10.98
	1.5	-2.22	11.48
	1.6	-2.64	11.23
ARRAY2	2.1	-7.55	5.75
	2.2	-7.39	5.24
	2.3	-6.99	5.26
	2.4	-6.80	5.75
	2.5	-7.23	6.06
	2.6	-7.29	5.63
ARRAY3	3.1	-0.29	3.82
	3.2	-0.29	3.30
	3.3	0.21	3.14
	3.4	0.52	3.56
	3.5	0.22	3.99
	3.6	0.08	3.56
Additional wave gauges	probe	x(m)	y(m)
	g1	-1.82	13.31
	g2	-3.39	9.19
	g3	-5.50	6.20
Vectrino/ADV	x(m)	y(m)	z(m)
ADV1	-2.40	11.96	0.40
ADV2	-5.58	6.16	0.40
ADV3	-7.20	5.56	0.41
ADV4	-3.75	6.83	0.29
ADV5	-4.55	7.20	0.11

Table 2. Sequence of the first tests and test parameters.

Date	Test	d [m]	Hm_0 [m]	Tp [s]	Dir [º]	Spread [º]
	13		0.100	1.19		
01-11-2017	14	0.60	0.150	1.45	40	0
	15		0.175	1.57		
	16		0.200	1.68		
	17		0.100	1.19		
02-11-2017	18	0.60	0.150	1.45	65	0
	19		0.175	1.57		
	20		0.200	1.68		
	21		0.100	1.19		
03-11-2017	22	0.60	0.150	1.45	90	0
	23		0.175	1.57		
	25		0.200	1.68		

3. NUMERICAL MODEL

3.1. Numerical Solver

OpenFOAM® is a widely used open source C++ toolbox, which includes different solvers, tools and libraries. It includes the solver interFoam and several boundary conditions, specially designed for coastal processes within IHFOAM. Numerical simulations have been performed using a suite of tools which includes boundary conditions (waves, currents and waves&currents) (Higuera *et al.*, 2013, DiPaolo *et al.*, 2021) and porous media solvers (Romano, 2020) for coastal and offshore engineering applications. It can solve both three dimensional Reynolds Averaged Navier Stokes equations (RANS) and Volume Averaged Reynolds averaged Navier Stokes equations (VARANS) (Higuera *et al.*, 2013) for two phase flows. As it is described in Romano *et al.* (2020), the VARANS equations allow to model the flow inside a porous material, which is modelled as a continuous media. The mass and the momentum conservation equations, coupled to the VOF equation, read as follows:

$$\frac{\partial u_i}{\partial x_i n} = 0$$

$$(1+c)\frac{\partial p u_i}{\partial t \; n} + \frac{u_j}{n}\frac{\partial p u_i}{\partial x_j n} = -g_j x_j \frac{\partial \rho}{\partial x_i} - \frac{\partial p^*}{\partial x_i} -$$

$$\frac{\partial}{\partial x_j}\mu_{eff}(\frac{\partial \rho u_i}{\partial x_j n} + \frac{\partial \rho u_j}{\partial x_i n}) + A u_i - B|u_i|u_i$$

$$\frac{\partial \alpha}{\partial t} + \frac{\partial u_i \alpha}{\partial x_i n} + \frac{\partial u_{ci}\alpha(1-\alpha)}{\partial x_x n} = 0$$

where u_i is the velocity (m/s), x_i the Cartesian coordinates (m),

g_j the components of the gravitational acceleration (m/s²), n(-) is the porosity, ρ the density of the fluid (kg/m³), p^* the ensemble averaged pressure in excess of hydrostatic, defined as $p^* = p - \rho \, g_j \, x_i$ (Pa), being p the total pressure, α the volume fraction indicator function (-) , which is assumed to be 1 for the water phase and 0 for the air. μ_{eff} is the effective dynamic viscosity (Pa s) that is defined as $\mu_{eff} = \mu + \rho v_t$ and takes into account the dynamic molecular (μ) and the turbulent viscosity effects (ρv_t); v_t is the eddy viscosity (m²/s), which is provided by the turbulence closure. u_{ci} is the compression velocity. Following the work by Van Gent (1995), the expressions for A, B, and C are as follows:

$$A = a\frac{(1-n)^2}{n^2}\frac{\mu}{D_{50}^2}$$

$$B = b(1 + \frac{7.5}{KC})\frac{1-n}{n^3}\frac{\rho}{D_{50}}$$

$$C = \gamma\frac{(1-n)}{n}$$

where D_{50} (m) is the mean nominal diameter of the porous material, KC (−) the Keulegan-Carpenter number, a (−) and b (−) are empirical nondimensional coefficients and y=0.34 (−) is a nondimensional parameter.

No turbulence model was considered in this preliminary study.

3.2. Numerical Set-up

The wave tank dimensions are 39.23 m x 18.6 m x 2 m and the total wavemaker length is 28.8 m resulting from 72 paddle wave boards with a 0.4 m width in the 39.23 m side and almost centered in it (5 m + 28.8 m + 5.43 m). Following guidelines of having 7 to 10 cells across the wave height and 100 cells along the wave length, values of dx = dy = 0.02 m to 0.035 m and dz = 0.01 m were reached, as in tests periods varied from 1.19 s to 1.68 s and wave lengths from 2.093 m to 3.5 m. The geometry of the breakwater and the wave tank was constructed in SALOME-9.2.2, and the generated stl ("stereolithography") files were used to define boundaries and to construct the mesh using either fvmesh or snappyHexMesh tool.

Refinements parameters near the paddleboards, the breakwater and the lateral walls were defined in snappyHexMesh Dictionary, using 2 levels for every surface-based refinement and 3 cells between levels. The 9.2 M cells in the domain are mainly composed by cubes. Figure 2 shows a top view of the wave tank and a detail of the mesh around the breakwater.
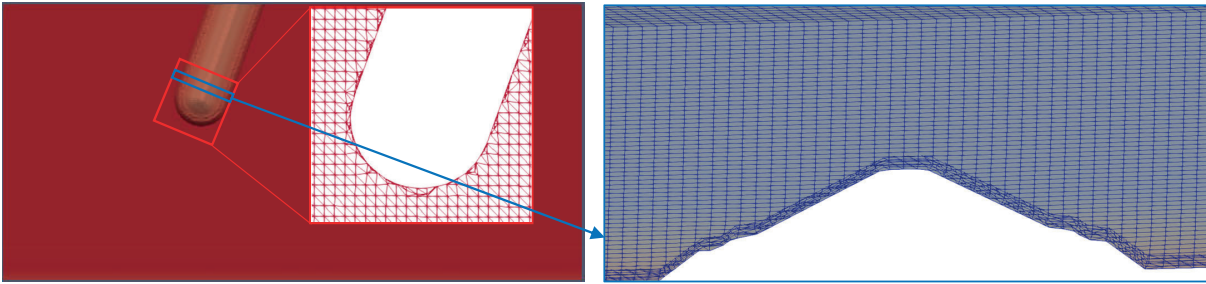
Figure 2. Overview of the tank with breakwater mesh and detail of two slices.
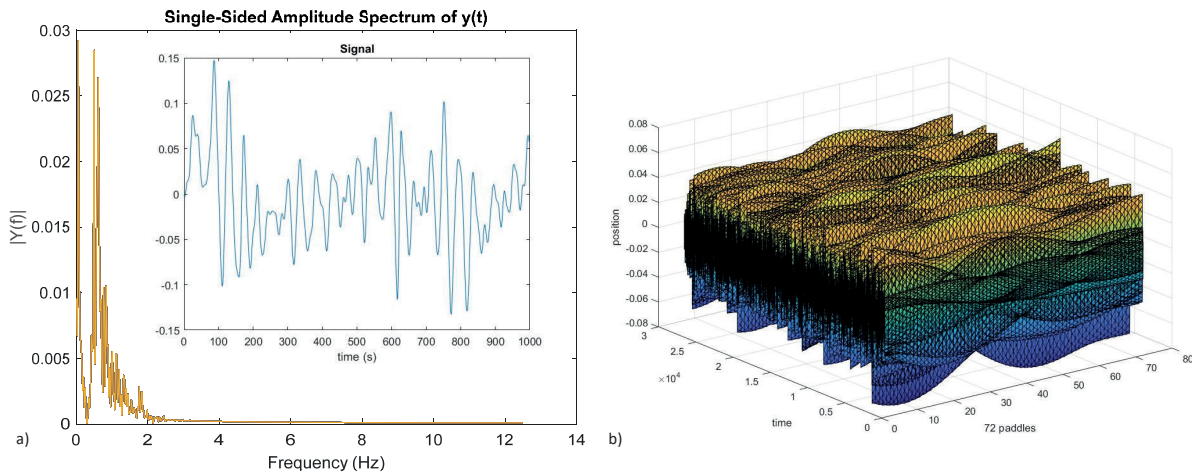
Figure 3. Waves generated by the 72 paddles in test 17: a) Jonswap spectrum; b) data for all boards.

4. NUMERICAL SIMULATIONS RESULTS VERSUS EXPERIMENTAL RESULTS

Figure 4 shows numerical simulations for different irregular wave train angles, 40º, 65º and 90º. Figure 5 and 6 show numerical simulations for incident irregular wave train angle of 65º, and different heights, T18 and T19, and results for incident irregular wave train angle of 90º, T25 (see Table 2).

It is clearly observed that the intended direction, 40º for T13, 65º for T18 and T19 and 90º for T25 was attained. It can be also verified that the waves reach breakwater in a few seconds, causing reflection but keeping a clean wave train in T18 until 40 s but generating a local area behind the breakwater with some dispersion. A higher wave amplitude for the same direction (T19 as compared with T18) induces higher velocities at the surface and near the breakwater surface, as expected, as well as interferences appear along the tank sooner, which looks higher in the upstream face.

On the other hand, extreme oblique waves (90º, T25), perpendicular to the breakwater, even with a higher wave train seems to induce less perturbation around the breakwater. Figure 7 shows T25 experimental data along time of free-surface location at all acoustic wave probes (see Figure 1 and Table 1 - Array1 (1.1 to 1.6), Array2 (2.1 to 2.6) and Array3 (3.1 to 3.6), g1, g2 and g3) and velocity data at all Vectrinos (ADV1 to ADV5). Figure 8 illustrates variation along time, 0 to 30 s, of instantaneous velocities experimental measurements and numerical simulation results, both at ADV3, which is located in the front of the breakwater's trunk armour (see Figure 1) as well as of water depth at 5 acoustic wave probes, at the three individual probes and at the Arrays (one location of the 6 in each Array). Figure 9 shows statistics results by means of boxplots for the water depth and for the velocity data at the same incident irregular wave train angle of 90º (T25), for both set of data, experimental and numerical, respectively. Figure 10 illustrates histograms for the same data.
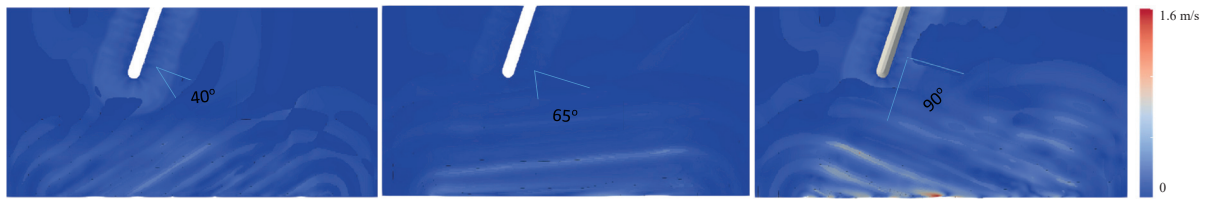
Figure 4: Snapshots of the numerical simulations, showing velocity magnitude (0 to 1.6 m/s) on free-surface and around the breakwater for incident irregular wave train angle at t=6s for: a) 40°: T13; b) 65o: T19; and c) 90°: T25.
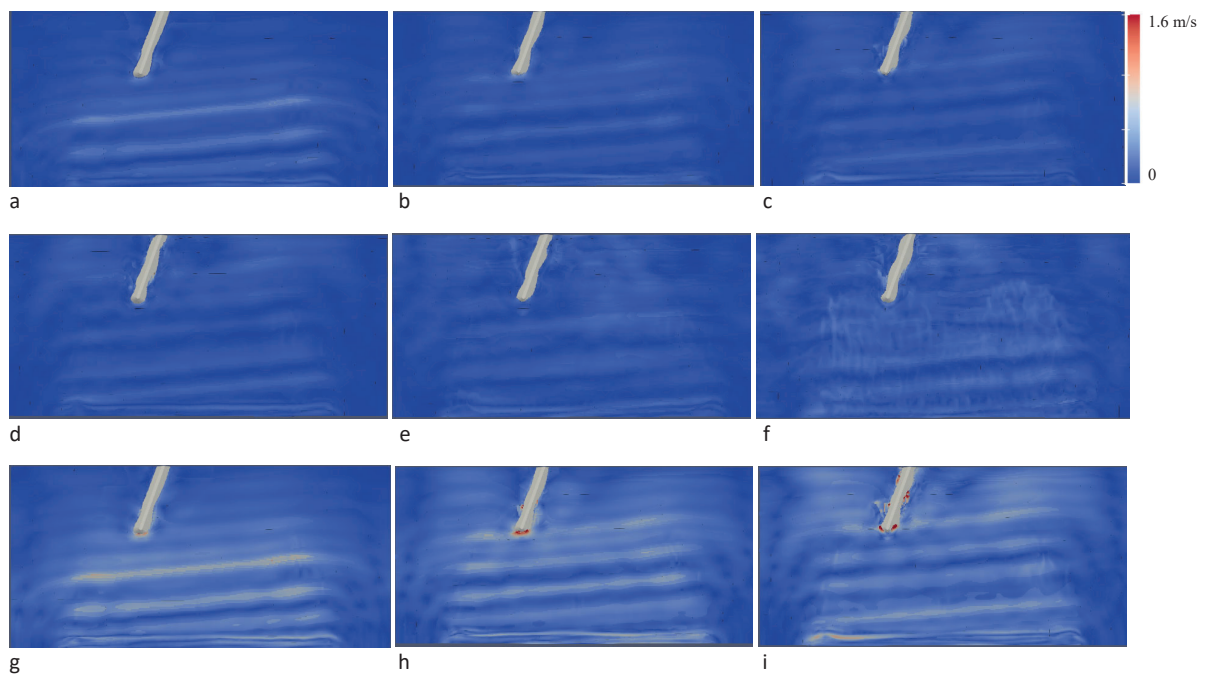
Figure 5: Snapshots of the numerical simulations, showing velocity magnitude (0 to 1.6 m/s) on free-surface and around the breakwater for incident irregular wave train angle of 65o: T18 for t=10 s, 12 s, 14 s, 20 s, 30 s and 40 s (a to f) and T19 for t=10 s, 12 s and 14 s (g to i)
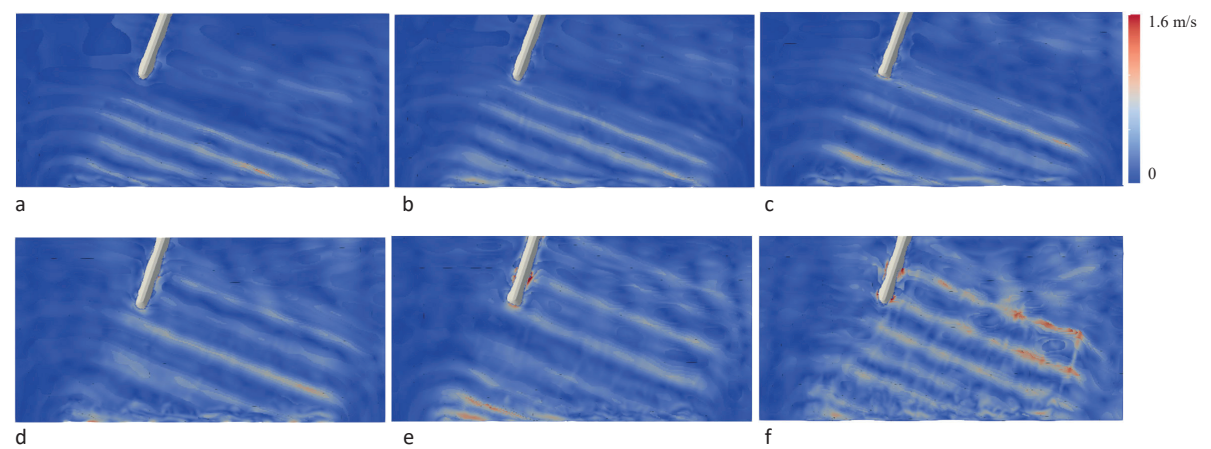
Figure 6: Snapshots of the numerical simulations, showing velocity magnitude (0 to 1.6 m/s) on free-surface and around the breakwater for incident irregular wave train angle of 90°: T25 for t=10 s, 12 s, 14 s, 17.5 s, 20s and 30s (a to f) .
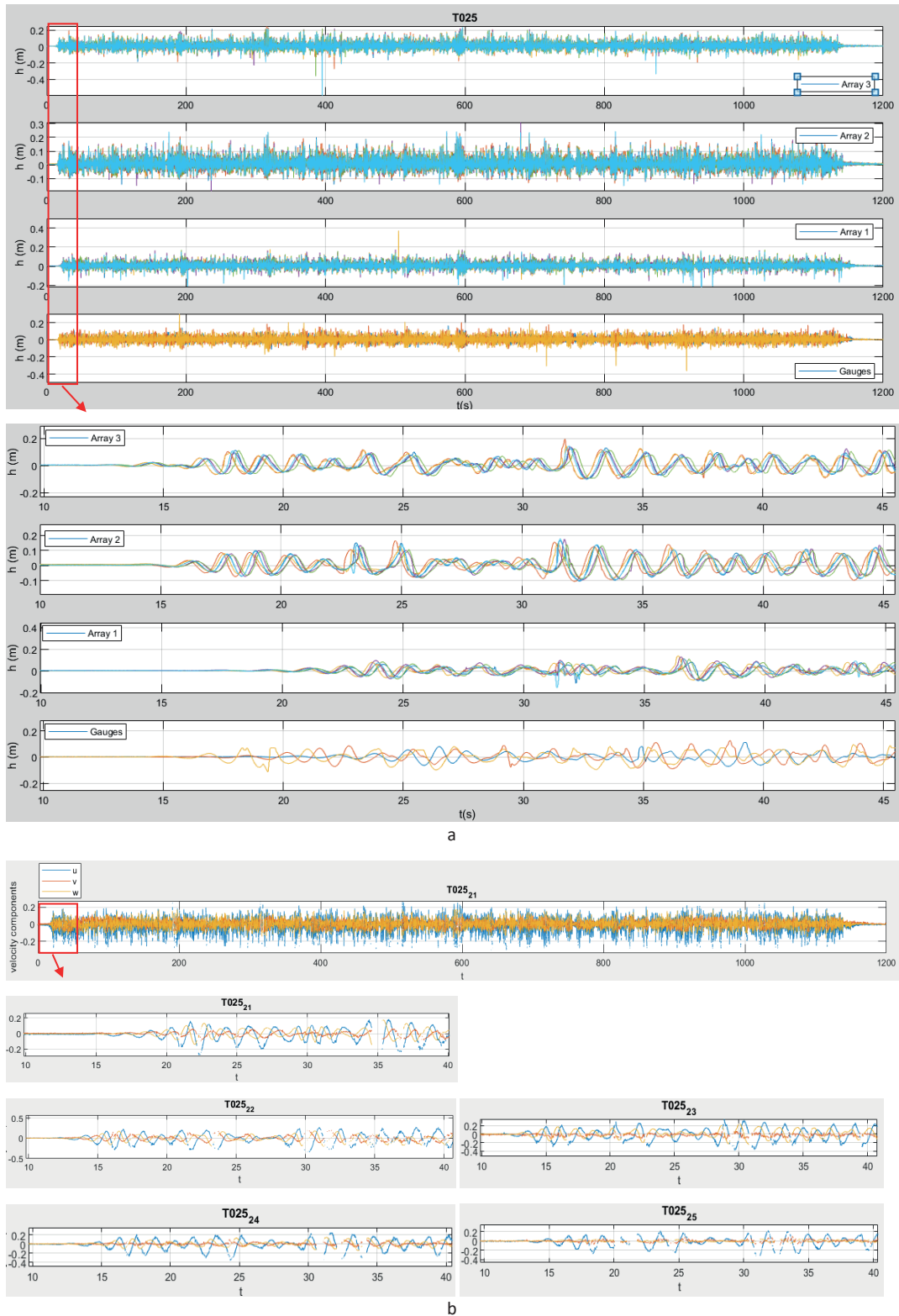
Figure 7: Experimental data for incident irregular wave train angle of 90º, T25: a) magnitude of the free-surface elevation at the different acoustic wave probes (Array1(1:6), Array2(1:6), Array3(1:6), g1, g2, g3) and b) velocity components data at ADV1 to ADV5.
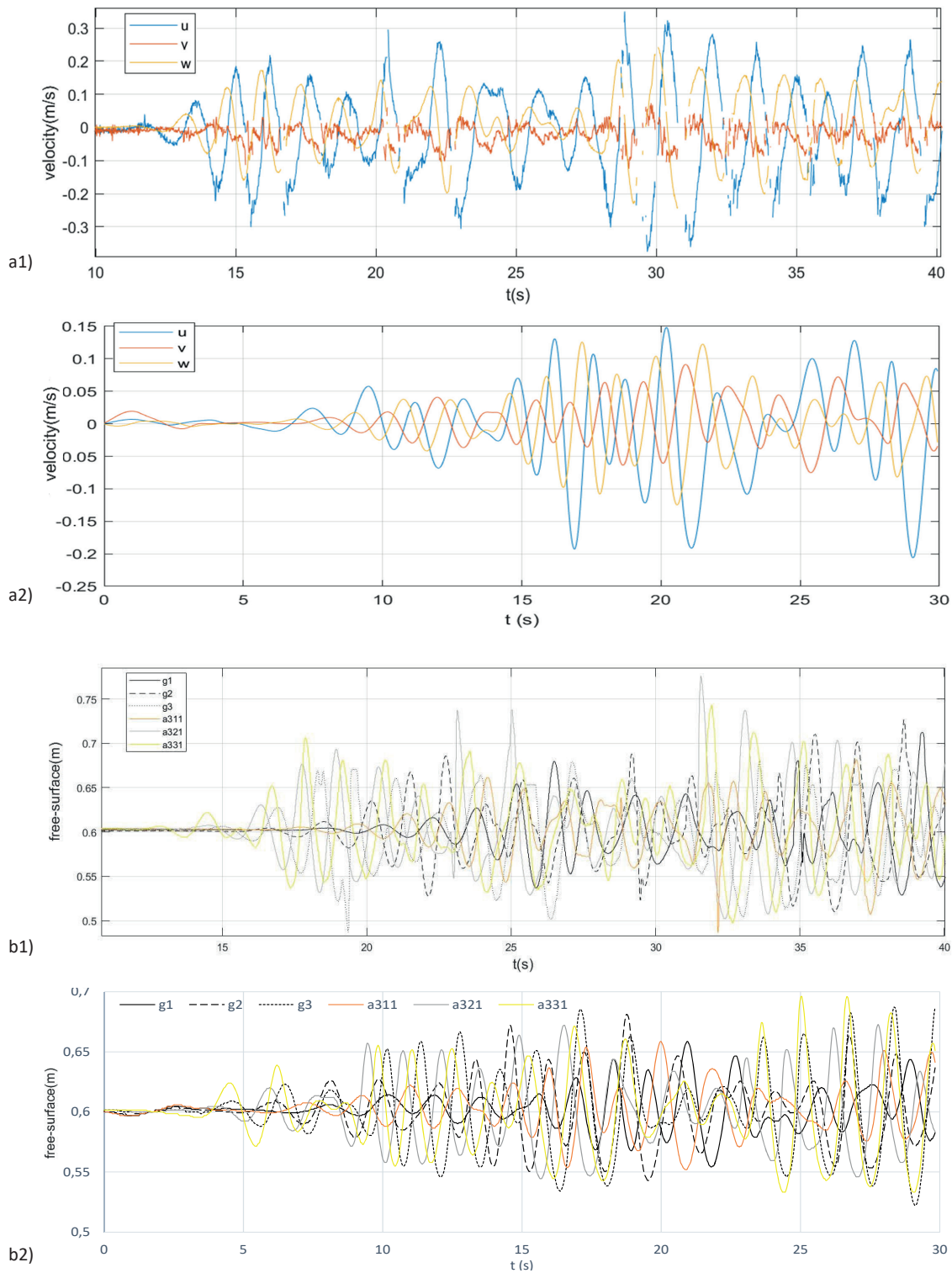
Figure 8: Velocity (a) and free-surface elevation (b) in different locations for incident irregular wave train angle of 90º, T25: a1) Vectrino experimental measurements – ADV3; a2) numerical simulation results at ADV3 location point; b1) experimental measurements at 5 acoustic wave probes; b2) numerical simulation results at the 5 acoustic wave probe locations.
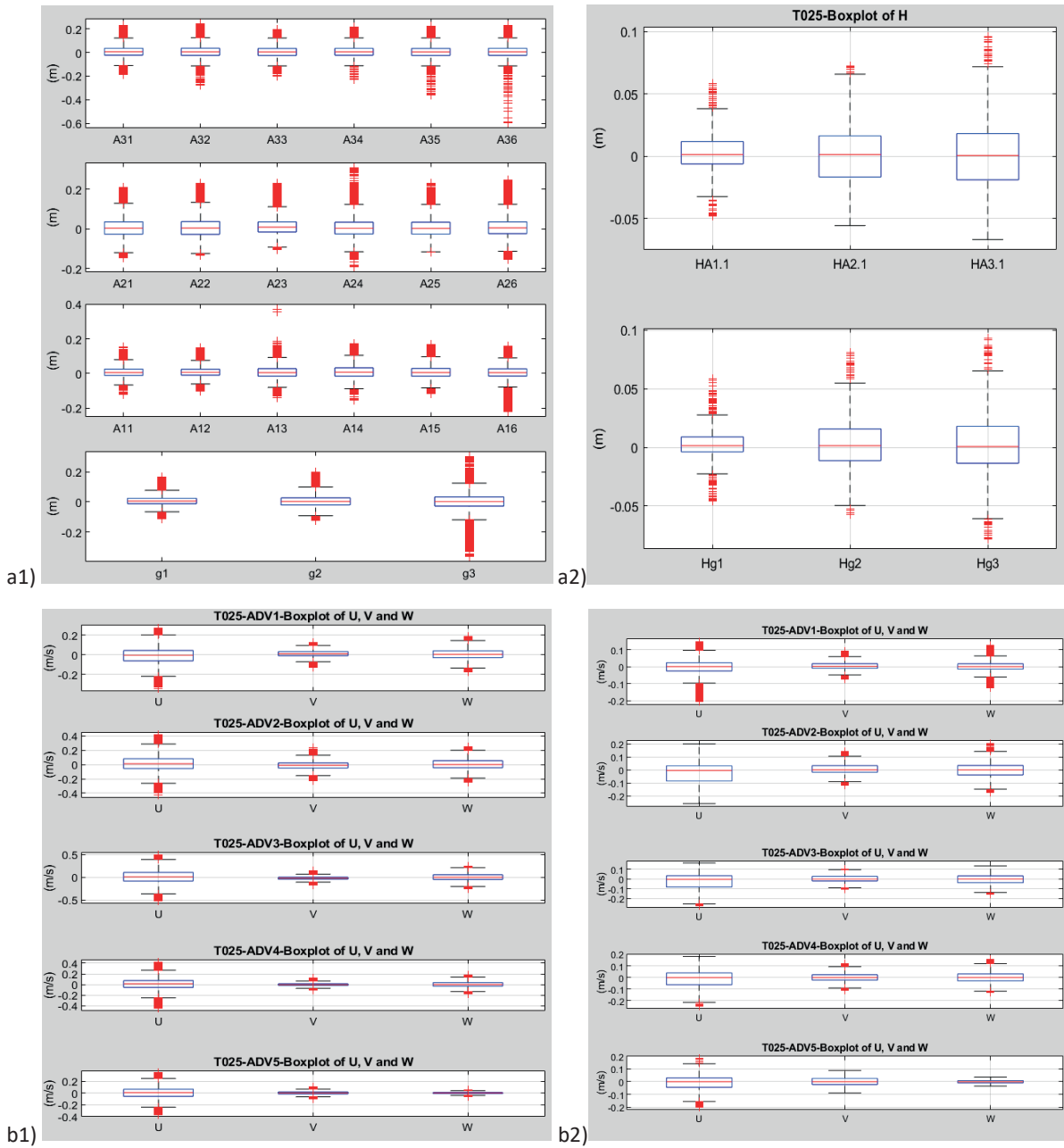
Figure 9: Basic statistics for experimental data (a1 and b1) and numerical simulation results (a2 and b2) of the free-surface elevation at the different acoustic wave gauge locations (a) and velocity at ADVs/Vectrinos locations (b) for incident irregular wave train angle of 90º, T25.
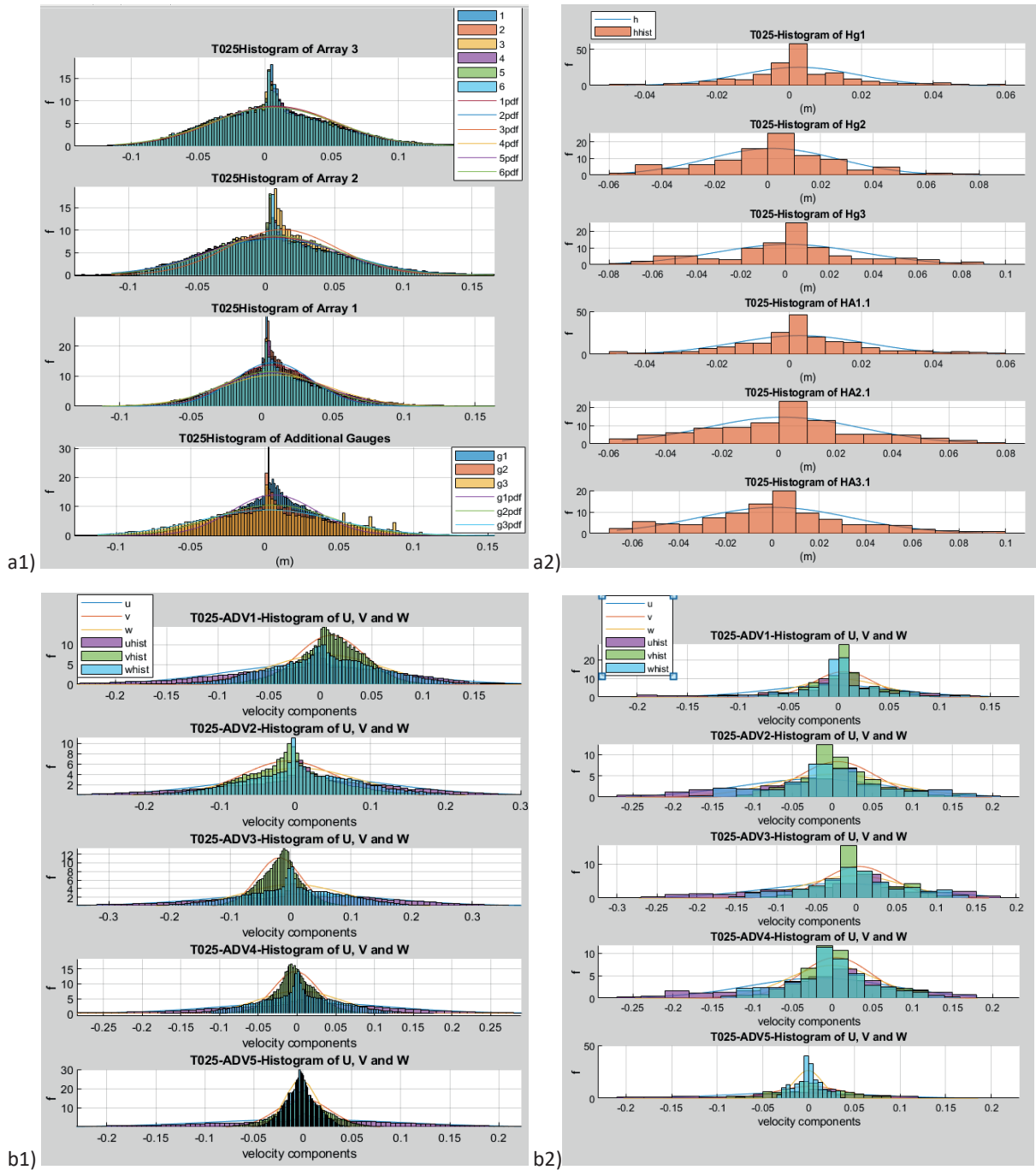
Figure 10: Distribution of experimental data (a1 and b1) and Numerical simulation results (a2 and b2) of the free-surface elevation at the different acoustic wave gauge locations (a and b) and velocity components in the different Vectrinos locations (c and d) for incident irregular wave train angle of 90°: T25.

5. DISCUSSION

Numerical and experimental results cannot be directly compared for two reasons: 1) synchronization of results is not exact as velocities experimental data was stored in a different computer, being the Vectrinos commanded manually; also in the numerical model a ramp of 2 s was considered; 2) data provided by measurements and numerical simulations are not in the same time steps as the dynamical adjustable time step was required for a better performance of the numerical simulations, the numerical model just ran for 30 s while experiments lasted 1200 s, and not all the results values could be kept due to the enormous memory capacity needed to store (30 s x 3142939) x 300 Hz for water depth and (30 s x 3142939) x 100 Hz for velocities. For a given time, numerical results are just 1/3 of the experimental velocities data and 1/10 of the water depth experimental data. Although numerical and experimental data cannot be directly compared, numerical results can be evaluated based on experimental data. Because of a shorter numerical analysis period compared to the experimental one, it is natural that the result ranges of both free surface and velocity data are lower than the experimental range. In fact, from the analysis of Figure 7, positive and negative peaks can be observed occasionally, which could never be predicted when analysing a shorter period. However, even for the analysis of equal period, for example from 15 s to 30 s to avoid influence of the numerical ramp, experimental data reaches higher maximum values and lower minimum values both for free-surface variation and velocity (Figure 8).

In Figure 8, just a location of 1 of the 6 probe per Array was considered because the difference between the values of the water elevation for probes of the same Array is not significant for the present analysis (Figure 7a). Concerning velocity data, it can be observed that the quality is good since most of the values were retained after filtration (Figure 7b).

Experimental velocity data show some small variations of high frequency, which are not detected by the present numerical model (Figure 8a), which was expected not only by the nature of the numerical model used, but also because the number of time intervals analysed for numerical data are smaller than the experimental data.

The model is based on the Navier-Stokes equations and the calculation considers finite volumes greater than necessary to detect turbulence. Apart from this, the variation along time for each probe is similar in experimental and numerical data sets.

Free-surface elevation ranges as well as velocities ranges are comparable in most locations. Some discrepancies were observed in negative velocities at the front of the breakwater's trunk armour (ADV3) and in the highest values of free-surface in Array2, probe 3.2.1.

Figure 9a illustrates both predicting a larger free-surface elevation range for g3 and a lower for g1 as well as in the arrays, a larger for 3 and a lower for 1, being g3 and array 3 closer to the breakwater round head.

Figure 9b shows a larger velocity range for u component (breakwater axis direction) and a lower for v component. U component range is larger for ADV3 and ADV2, which are closer to the breakwater head, followed by ADV4 and ADV5. ADV2, 3 and 4 are approximately equidistant from the breakwater but ADV5 is closer to the breakwater. Concerning W component, the range is larger for ADV2 and lower at ADV5.

Figure 10 shows apart from the higher frequency of the mean value a distribution of free-surface elevation and of velocity not far from gaussian in the remaining range. Free-surface elevation for Array1 and 2 shows different distribution for each probe of the array. However, the distribution of free-surface elevation for the probes in Array 3 are similar. This could also be observed in Figure 9, where different peaks are represented.

6. CONCLUSIONS

Experimental trials were carried out under the RodBreak project to generate different extreme wave conditions (wave steepness of 0.055) with incident irregular wave train angles (from 40º to 90º) to reach breakwater. 3D wave tank simulations were performed using the OpenFOAM® v1812 model, reproducing for at least 30 s, the waves with different directions which were generated by the movement of the 72 paddle boards.

For each test, the movement of the boards in the physical model was defined in specific files to generate the corresponding irregular wave train with a multi-paddle dynamic boundary condition. Numerical results show the different waves at various incidence angles as desired, showing absorption on the side and front walls as expected. This avoids the modification of boundaries to be perpendicular to the wave direction, which is relevant in the case of extreme oblique waves as the modification implicates a significant change of the tank dimensions. However, changing domain dimensions is irrelevant in real cases and could be an interesting way to produce a wave train.

Analysis of the generated wave train, direction, water depth and local velocity data based on numerical simulations were done as well as on experimental data. In spite of numerical analysis being based on a shorter period with less time intervals, which gave obvious differences, both sets of data conduct to consistent observations. Larger variations occur in the proximity of the breakwater head, which is consistent with the observation and with the occurrence of the largest movement in the breakwater blocks. It can be said that good results were obtained.

It is soon intended to perform different and detailed analysis of the action of the different irregular wave train on the breakwater as well as the analysis of their reflection on the breakwater.

ACKNOWLEDGEMENTS

REFERENCES

Brackbill, J.U.; Kothe, D.B.; Zemach, C. (1991). A continuum method for modeling surface tension. J. Comput. Phys. 100, 335–354.

Carvalho, R.F.; Lemos, C.M.; Ramos, C.M. (2008). Numerical computation of the flow in hydraulic jump stilling basins, Journal of Hydraulic Research 46(6):739-752

Goring, D.G.; Nikora, V.I. (2002). Despiking acoustic Doppler velocimeter data. Journal of Hydraulic Engineering, 128(1):117-126.

Higuera, P.; Lara, J.L.; Losada, I.J. (2013). Realistic wave generation and active wave absorption for Navier-Stokes models. Application to OpenFOAM® R. Coastal Engineering, 71:102-118.

Higuera, P., Lara, J.L. & Losada, I.J., Three-dimensional numerical wave generation with moving boundaries. (2015). Coastal Engineering [Vol.101, pp. 35-47]

Hirt, C.W.; Nichols, B.D. (1981). Volume of fluid (vof) method for the dynamics of free boundaries. J. Comput. Phys., 39, 201–225.

Jacobsen, N.G.; Fuhrman, D.R.; Fredsøe, J. (2012). A wave generation toolbox for the open-source CFD library: OpenFoam®. International Journal for Numerical Methods in Fluids, 70(9), 1073-1088

Lara, J.L., Higuera, P. Maza, M., Jesus, M. Losada, I.J., Barajas, G. (2012). Forces induced on a vertical breakwater by incidente oblique waves. 33rd. Int. Conf. on Coastal Engineering (ICCE), Santander, Spain.

Di Paolo, B.; Lara, J.L.; Barajas, G.; Losada, Í.J. .(2021) - Wave and structure interaction using multi-domain couplings for Navier-Stokes solvers in OpenFOAM®. Part I: Implementation and validation. Coast. Eng. 2020, 103799

Di Paolo, B.; Lara, J.L.; Barajas, G.; Losada, Í.J. (2021). Waves and structure interaction using multi-domain couplings for Navier-Stokes solvers in OpenFOAM®. Part II: Validation and application to complex cases. Coastal Engineering 164, 103818.(2021).

A Romano, JL Lara, G Barajas, Benedetto Di Paolo, G Bellotti, M Di Risio, IJ Losada, P De Girolamo (2020). Tsunamis Generated by Submerged Landslides: Numerical Analysis of the Near Field Wave CharacteristicsJournal of Geophysical Research: Oceans 125 (7), e2020JC016157.

Rusche, H. (2002). Computational Fluid Dynamics of Dispersed Two-Phase Flows at High Phase Fractions. Ph.D. Thesis, University of London, London, UK.

Santos, J.A.; Lemos, R.; Weimper, J.; Gronz, O.; Hofland, B.; Sande, J.; Pinheiro, L.; Spans, J.H.; Peña, E.; Reis, M.T.L.G.V.; Fortes, C.J.E.M.; Figuero, A.; Laiño, E.; Bornschein, A.; Kerpen, N.B.; Pedro, F.; Coimbra, M.; Körner, M.; van den Bos, J.; Dost, B.; Carvalho, R.; Alvarellos, A.; Pohl, R. (2019a). Data Storage Report. RODBreak - Wave run-up, overtopping and damage in rubble-mound breakwaters under oblique extreme wave conditions due to climate change scenarios. https://doi.org/10.5281/zenodo.3355657.

Santos, J.A.; Pedro, F.; Coimbra, M.; Figuero, A.; Fortes, C.J.E.M.; Sande, J.; Körner, M.; Lemos, R.; Bornschein, A.; Weimper, J.; van den Bos, J.; Dost, B.; Hofland, B.; Carvalho, R.; Alvarellos, A.; Peña, E.; Pohl, R.; Kerpen, N.B.; Reis, M.T.L.G.V. (2019b). 3-D scale model study of wave run-up, overtopping and damage in a rubble-mound breakwater subject to oblique extreme wave conditions. Defect and Difusion Forum, 396:32-41.

Weisse, R.; Bellafiore, D.; Menendez, M.; Mendez, F.; Nicholls, R.J.; Umgiesser, G.; Willems, P. (2014). Changing extreme sea levels along European coasts. Coastal Engineering, 87:4-14.

Weller, H.G. (2008). A New Approach to Vof-Based Interface Capturing Methods for Incompressible and Compressible Flows; Report TR/HGW/04; OpenCFD Ltd.: London, UK.